

Band structure engineered layered metals for low-loss plasmonics

Morten N. Gjerding and Kristian S. Thygesen*

*Center for Atomic-scale Materials Design (CAMD) and Center for Nanostructured Graphene (CNG),
Department of Physics, Technical University of Denmark,
Anker Engelundsvej 1, 2800, Kgs. Lyngby, Denmark*

Mohnish Pandey

*Center for Atomic-scale Materials Design (CAMD),
Department of Physics, Technical University of Denmark,
Anker Engelundsvej 1, 2800, Kgs. Lyngby, Denmark*

(Dated: November 28, 2021)

Plasmonics currently faces the problem of seemingly inevitable optical losses occurring in the metallic components that challenges the implementation of essentially any application. In this work we show that Ohmic losses are reduced in certain layered metals, such as the transition metal dichalcogenide TaS₂, due to an extraordinarily small density of states for scattering in the near-IR originating from their special electronic band structure. Based on this observation we propose a new class of band structure engineered van der Waals layered metals composed of hexagonal transition metal chalcogenide-halide layers with greatly suppressed intrinsic losses. Using first-principles calculations we show that the suppression of optical losses lead to improved performance for thin film waveguiding and transformation optics.

INTRODUCTION

The basic idea of plasmonics is to utilise the sub wavelength confinement of light on metallic surfaces in the form of plasmon-polaritons to enable a range of applications including negative index materials[1], imaging[2–4], energy conversion[5, 6], quantum information processing[7] and transformation optics[8, 9]. However, in practice many of these applications are challenged by optical losses occurring in the metallic components [10–12]. So far, no viable alternatives to the noble metals have been found and the detrimental losses have appeared to be an unavoidable property of any conducting material.

Optical losses in metals originate from electronic transitions between the occupied and unoccupied parts of the crystal band structure, see Figure 1. In the absence of any scattering mechanisms, absorption of photons can take place only via vertical transitions in the Brillouin zone due to the small momentum of the photon, cf. transition (iii). However, scattering on crystal imperfections, phonons or other electrons, can provide the extra momentum required for light absorption via non-vertical electronic transitions, cf. transitions (i) and (ii). Typically, losses increase significantly above the onset of interband transitions which sets a hard upper limit on the operating frequencies of a plasmonic material. The effect of intra-band scattering (transition (ii)) on the optical properties of metals is often accounted for by a phenomenological relaxation time. As we show here, a key to describe and discover intrinsic low-loss metals is to move beyond the commonly used constant relaxation time approximation and include band structure effects in the scattering rate.

Previous searches for new plasmonic materials in

the optical regime have explored the alkali-noble intermetallics[13, 14] and transition metal nitrides[15]. Some materials showed promise although their performance was still lower than that of the noble metals. Because all optical losses ultimately depend on the existence of an initial occupied and final unoccupied electronic state, one strategy for reducing losses has been to reduce the number of states available for scattering. Following this principle, doped semiconductors and transparent conducting oxides have been proposed for applications in the mid and near-infrared, respectively[16]. Recently, graphene plasmonics has been extensively studied due to its low density of states around the Dirac cone and easily tuneable plasma frequency[17, 18].

The 'elusive loss-less metal'[19] represents the ideal plasmonic material where no states are available for scattering in a particular frequency range thus eliminating optical losses completely, cf. transition (iv) in Figure 1. Such a metal is obtained when the metallic, i.e. partially filled, band(s) are separated from all higher and lower lying bands by sufficiently large energy gaps. Metals with such isolated intermediate bands are very rare among the conventional bulk materials. On the other hand, low-dimensional materials, in particular layered materials, with a significant fraction of under-coordinated atoms and thus overall weaker hybridization, might be more likely to exhibit such characteristic band structures.

In this paper we test this hypothesis by examining the computed band structures of the metallic layered materials identified in Ref. [20]. We discover that the transition metal dichalcogenides (TMDs) TaS₂ and NbS₂ as well as aluminum(II) chloride, AlCl₂, have monolayer band structures that resemble that of the 'elusive loss-less metal', and confirm by first-principles calculations that the special electronic structure does entail lowered

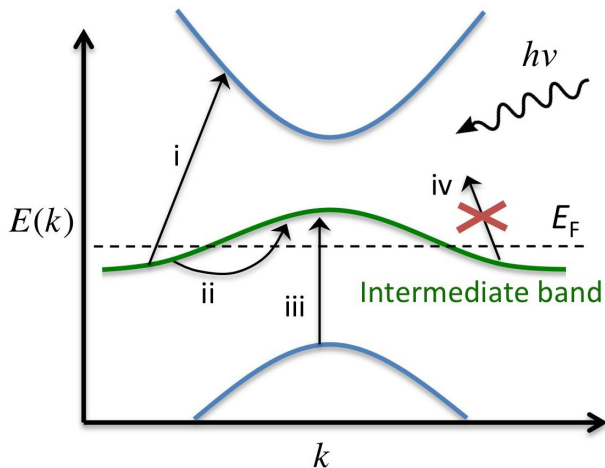


FIG. 1. **Origin of optical losses in metals.** The optical loss in metals originate from electronic transitions from occupied to unoccupied states in the crystal band structure (i, ii, iii). Only vertical transitions (iii) are allowed if scattering mechanisms are disregarded. Scattering mechanisms (impurity scattering, phonon absorption and emission, electron-electron scattering) can give the momentum required to allow for indirect transitions (i, ii). A metal with an intermediate band separated by gaps will suppress the number of transitions available (direct and indirect) at specific frequencies like in (iv) where no unoccupied state exists. When the gaps are sufficiently large to separate intraband(i) from interband(ii, iii) losses, some spectral ranges become immune to all quasi-elastic loss mechanisms.

optical losses. The constant relaxation time approximation is shown to be insufficient for describing the optical permittivity of these materials and we propose a simple model of the scattering rate based on the joint density of states to remedy this deficiency. Based on the promising results obtained for the TMDs we propose a new class of bandstructure engineered layered materials composed of transition metal chalcogenide-halide layers that greatly suppress the optical losses, and demonstrate the improved performance of these materials for thin film waveguiding and transformation optics.

RESULTS

Identifying low loss layered metals. Examining the computed band structures of the metallic layered materials identified in Ref. [20] by data filtering the Inorganic Crystal Structure Database (ICSD, Sec. S1) reveal that the transition metal dichalcogenides (TMDs) 2H-TaS₂ and 2H-NbS₂ as well as aluminum(II) chloride, AlCl₂, have monolayer band structures that resemble that of the 'elusive loss-less metal'. While 2H-TaS₂ and 3R-NbS₂ have been synthesized in bulk form, AlCl₂ was derived from the experimentally known AlCl₃ by removing an interstitial Cl layer.

Figure 2 shows the atomic structures, band structures, and density of states (DOS) for (a) 2H-TaS₂, (b) 3R-NbS₂, and (c) 1T-AlCl₂. The band structures of the monolayers are shown (red) although we will focus on the bulk structures throughout this work. In the case of 2H-TaS₂ and 3R-NbS₂ the formation of the bulk from the monolayer breaks the degeneracy of the highest valence band at the Γ point and closes the gap to the metallic band, but the DOS above and below the intermediate band remains fairly low. Inter-layer hybridization plays a smaller role for 1T-AlCl₂; in particular, the band gaps are present for both the monolayer and bulk. The metallic band in AlCl₂ is formed by the Al *s*-states, and the small band width of 1 eV is a consequence of the weak hybridization between the Al atoms within the same atomic plane with the Cl atoms acting mainly as spacers. We stress that AlCl₂ is thermodynamically unstable. Although its calculated heat of formation is negative (-0.89 eV/atom) relative to the standard states of Al and Cl, it lies 0.7 eV above the 'convex hull' when considering other competing phases (see Methods). In contrast, the layered compound AlCl₃ is stable and has been experimentally synthesised. Starting from AlCl₃ it may be feasible to remove the loosely bound Cl interstitial layer and thereby form metastable AlCl₂.

We verify that the gapped metallic band structures entail lowered optical losses by performing first-principles calculations to obtain the dielectric function of AlCl₂ with an Al vacancy introduced in a 3x3x2 supercell. The introduction of a vacancy is necessary to probe the optical losses due to intraband transitions where the defect provides the required momentum, see Figure 1, transition ii. (Qualitatively similar results would be expected from phonon or electron scattering, however, such processes are more complicated to describe from first principles.) For comparison, a similar calculation was performed for a 3x3x3 supercell of Ag with a single vacancy (see Methods). Figure 3 (full lines) shows the imaginary part of the dielectric function which is directly related to the optical losses of the metal. Optical losses at low frequencies due to the intraband transitions are indeed observed.

The dielectric function of a metal can be divided into contributions from interband and intraband transitions, respectively. It is customary to approximate the latter by a Drude response:

$$\begin{aligned} \epsilon(\omega) &= \epsilon_{\text{inter}}(\omega) + \epsilon_{\text{Drude}}(\omega), & (1) \\ \epsilon_{\text{Drude}} &= 1 - \frac{\omega_p^2}{\omega^2 - i\omega\eta}, & (2) \end{aligned}$$

where ω_p is the plasma frequency and η is the constant relaxation rate of the free carriers. In Figure 3 we show the result of the Drude model (thick grey lines) with η fitted to obtain the best correspondence with the first-principles results using the bulk plasma frequency for ω_p . Excellent agreement is found for silver all the way

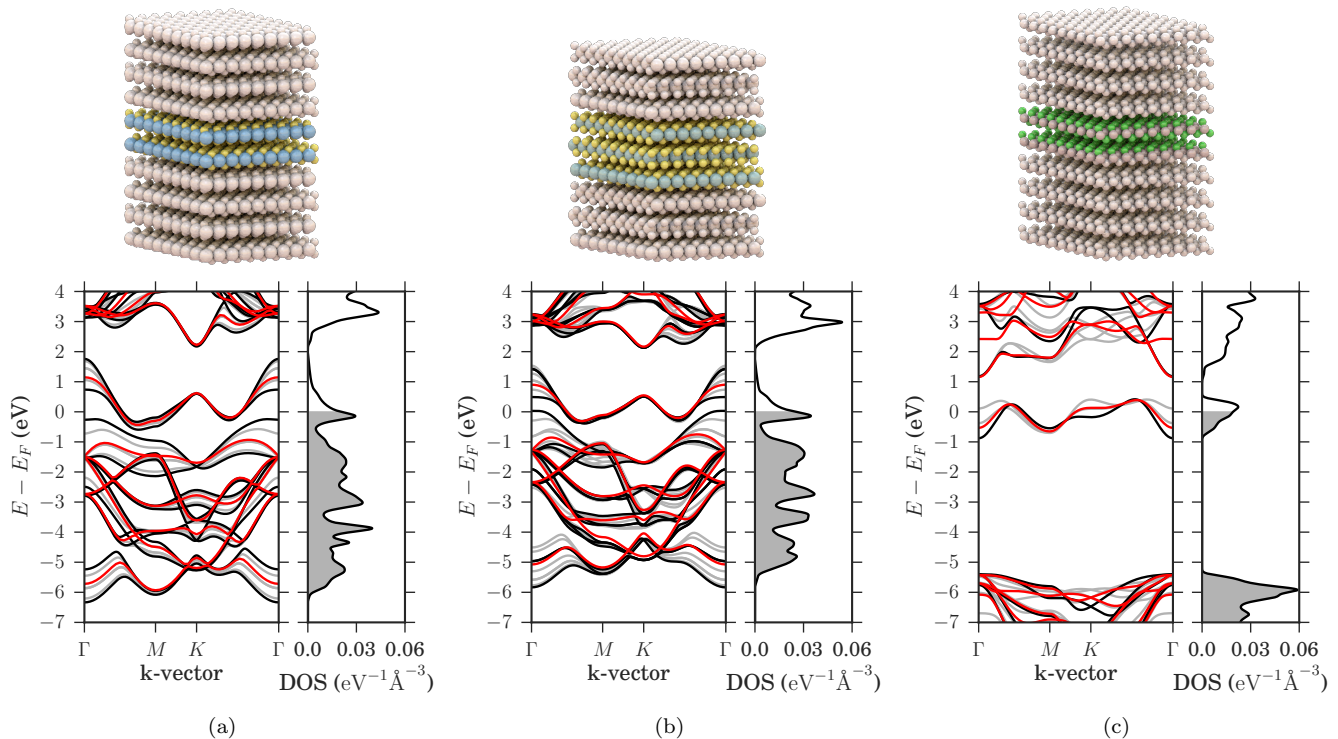


FIG. 2. **Band structures of vdW-metals.** (a) 2H(AA')-TaS₂, (b) 3R-NbS₂ have and (c) 1T-AlCl₂ exhibit special band structures where the metallic band is separated from higher and lower lying bands by finite energy gaps. Such band structures entail a strongly reduced number of states available for scattering as depicted in Fig. 1. Comparing the monolayer band structures (red lines) with the bulk band structures (black) reveal that inter layer hybridization break the valence band degeneracy at the Γ point for 2H-TaS₂ and 3R-NbS₂ and closes the gap below the Fermi level. The interlayer hybridization is non-essential for 1T-AlCl₂. The dispersion in the out-of-plane direction does not effect the existence of an intermediate band as evidenced by the grey lines showing band structures at band paths translated in the out of plane direction.

up to the onset of inter-band transitions demonstrating the validity of the constant relaxation time approximation for this material. In contrast, it is not possible to fit the dielectric function of AlCl₂ by the simple Drude model below the onset of interband transitions at 1.5 eV. This is a result of the special band structure of AlCl₂ which introduces a strong energy dependence of the joint density of states (JDOS). The JDOS gives the density of electron-hole pairs at a given frequency (disregarding momentum conservation) and thus represents the density of final states entering the expression for the scattering rate. In particular, the Drude model is not able to capture the strong reduction of the losses in the range 1-1.5 eV. In this energy range there are essentially no states available for scattering because of (i) the finite band width of the partially filled metallic band and (ii) the presence of band gaps separating the metallic band from the rest of the bands. Consequently, the JDOS will vanish at energies above the intraband transitions and below the onset of inter band transitions. In the case of AlCl₂, the band gaps are not large enough to completely separate the interband transitions from the intraband transitions, and consequently neither the JDOS nor $\text{Im}\epsilon$ become exactly

zero. However, the JDOS is strongly suppressed in the range 1-1.5 eV and this is the origin of the low-loss nature of AlCl₂.

Relaxation rate model. A more realistic description of the relaxation rate should include information about the number of available electron-hole transitions, i.e. the JDOS. A simple way to incorporate such a dependence is via

$$\eta(\omega) = a \frac{\text{JDOS}(\omega)}{\omega} \quad (3)$$

where a is a constant controlling the scattering strength. The expression can be motivated in different ways, but here it suffices to observe that (i) it reduces to the constant relaxation time approximation for a metal with a constant DOS in a region around Fermi energy (in which case the $\text{JDOS} \propto \omega$) and (ii) it correctly leads to a vanishing relaxation rate for energies where there are no final states for the scattering. As can be seen from Figure 3 (dashed lines) the model provides an excellent description of the optical losses of both materials. In the rest of the paper we use Eq. (3) to include scattering effects in a generic way setting the constant a to the same value for all materials. This value is chosen to reproduce the

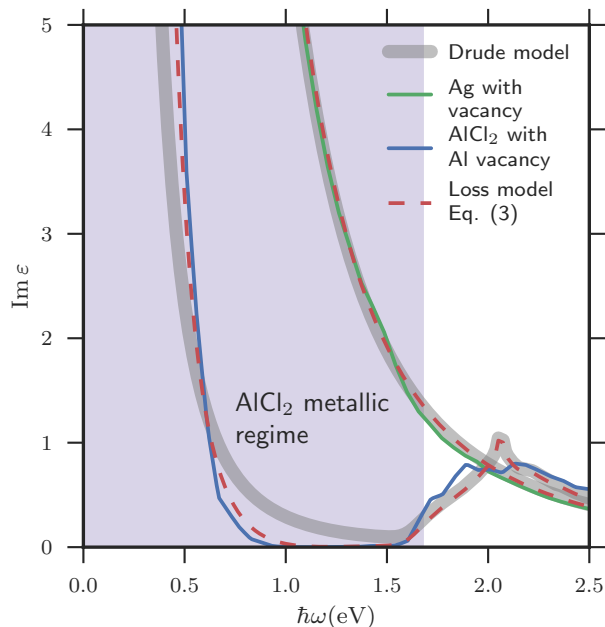


FIG. 3. **Defect induced optical losses and energy-dependent relaxation time model.** The calculated optical losses ($\text{Im}\epsilon$) for silver (green) and AlCl_2 (blue) with a vacancy defect. The thick grey line shows the standard Drude expression (2) with a constant relaxation time, $\tau = \hbar/\eta$, fitted to the ab-initio results. For silver this provides an accurate description of the low-frequency (intraband) losses while the description is less accurate for AlCl_2 where it misses the strong suppression of losses in the 1-1.5 eV range. Results of the Drude expression with the energy-dependent relaxation rate model (3) (dashed lines) are in excellent agreement with the ab-initio results for both systems.

experimental line width of the Ag surface plasmon (see Figure 4c).

We note that the JDOS model only accounts for first-order (quasi)-elastic scattering processes. Higher-order processes involving generation of several phonons or electron-hole pairs in one coherent photon-mediated event, could lead to absorption (loss) at energies between the intraband and interband transitions where the JDOS model would otherwise predict $\text{Im}\epsilon$ to vanish. We expect losses due to higher-order processes to be small in the near-IR and therefore neglect them in the following.

The potential of the vdW metals has been evaluated for two different plasmonic applications: Plasmonic waveguiding and transformation optics[22] discussed in detail below. The calculated dielectric functions, DOS, JDOS and relaxation rate η for all the layered metals studied in this work are provided in Sec. S9.

Plasmonic waveguiding. Plasmonic waveguides are envisioned as faster and less power consuming alternatives to the electronic interconnects currently used in integrated circuits. Essential prerequisites for such applications are long plasmon lifetimes and propagation lengths

as well as tight spatial confinement of the plasmon to interface efficiently with the nanometer scale electronic components[23]. To evaluate the potential of the layered metals for such applications we investigate plasmon propagation in 5 nm thin-film waveguides and single interface waveguides, respectively, see Figure 4(a-e). SiO_2 was used as the surrounding dielectric with a dielectric constant of $\epsilon = 2.1$ ($\lambda \sim 700$ nm).

Figure 4 shows the normalized propagation length, $\text{Re}(k_p)/\text{Im}(k_p)$, where k_p is the plasmon wave vector (b+c), the plasmon lifetime (c+g) and the mode extension into the dielectric (d+h), for silver, 2H-TaS₂, 1T- AlCl_2 , and the chalcogenide HfBrS, to be discussed later. The plasmon lifetime, τ , is calculated from the relationship $L = v_p\tau$ where v_p is the plasmon velocity (see Methods for details). The scattering strength (a) determining the frequency-dependent relaxation rate in Eq. (3) has been fixed by fitting the experimental result for the lifetime of the Ag surface plasmon.

For the thin film waveguide, only the symmetric plasmon mode was considered. The light-like anti-symmetric mode extends far into the dielectric with mode widths on the order of 1 micron in which case the requirement of small coupling to the environment is not fulfilled. For the single interface plasmonic waveguide silver shows significantly longer propagation lengths and lifetimes than any of the vdW metals. This is caused by the more efficient dielectric screening of Ag compared to the vdW metals, which implies that only a tiny fraction of the electromagnetic energy is contained within the silver surface, see Sup. mat. Fig. S1(a). The downside of the strong screening is the accompanying large mode widths caused by the electric field being pushed into the dielectric.

As the thickness of the thin-film plasmonic waveguide is reduced a larger fraction of the electric field is contained in the metal (Sup. mat. Fig. S1(b)) resulting in generally larger losses and decreasing plasmon group velocities[24]. Together these two effects combine to give superior propagation lengths, lifetimes and mode widths for the layered metals. The dependence of the plasmon lifetime on the intrinsic optical losses and the electric field distribution inside the metal is

$$\tau^{-1} \propto \int d\mathbf{r} |E_0(\mathbf{r})|^2 \text{Im}\epsilon. \quad (4)$$

From this it is clear that the relatively better performance of the layered metals in thin film waveguides as compared to Ag must be due to lower intrinsic losses because the electric field fraction within the vdW metal is much larger than in silver (Sup. mat. Fig. S1(b)).

It is well known that the PBE exchange-correlation (xc) functional underestimates both band gaps of semiconductors and interband transition energies in metals[25]. To test the influence of the xc-functional we have computed the dielectric function of 2H-TaS₂ using the range separated hybrid functional (HSE06) which

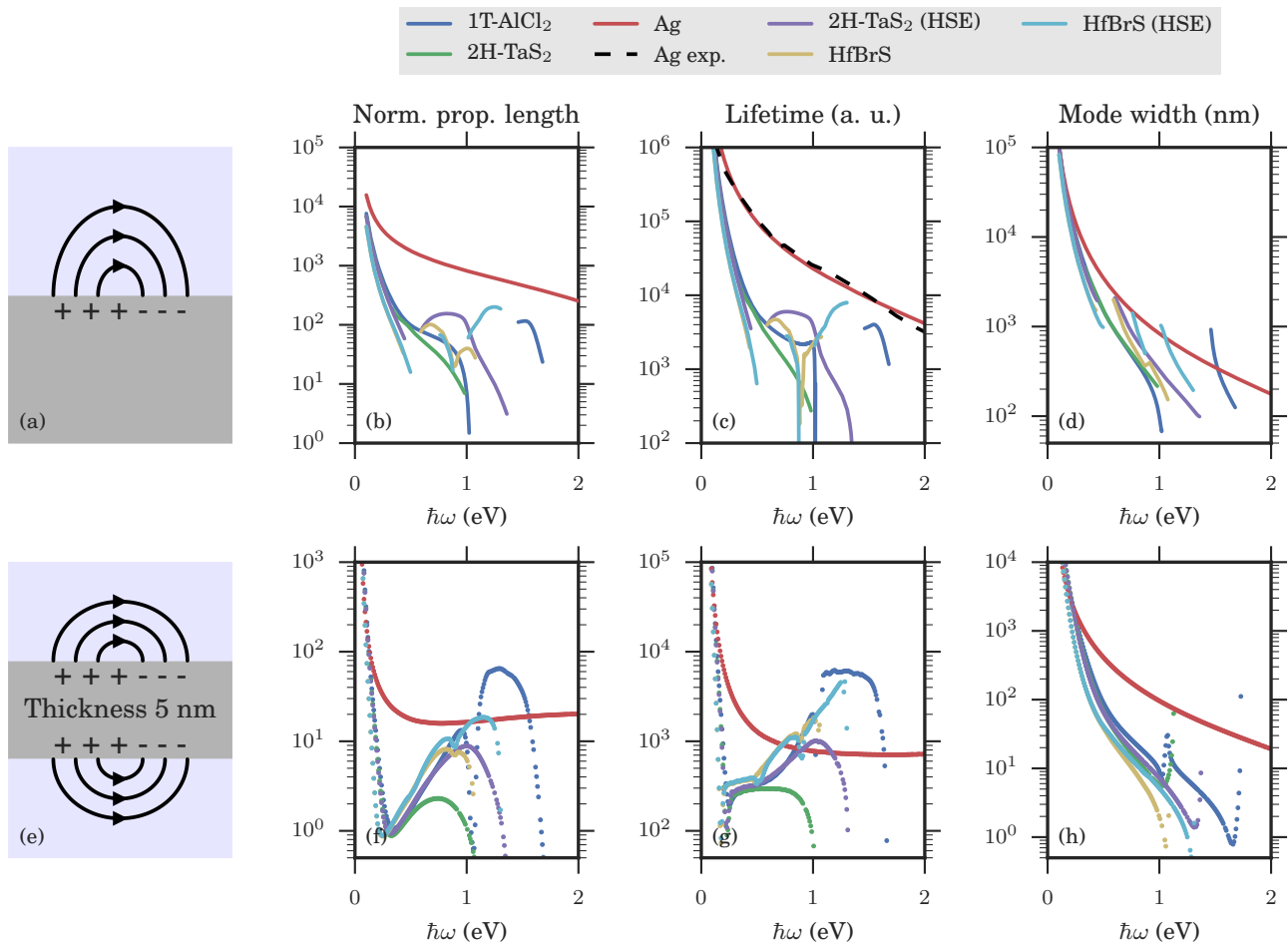


FIG. 4. **Plasmon waveguiding figures of merit.** The upper panels show the normalized plasmon propagation lengths $\text{Re}(k_p)/\text{Im}(k_p)$ (b), lifetimes (c) and mode width (d) for a plasmon on a single interface. The lower panels show the same results for a 5 nm thin film. The more efficient dielectric screening in silver reduces the fraction of the electric field located within the metal as compared to the case of the vdWH metals, resulting in lower losses, longer propagation lengths and lifetimes. On the other hand, since most of the electromagnetic energy is stored in the part of the electric field distributed over the dielectric, the mode widths of the surface plasmon becomes relatively large. Reducing the thickness of the metal to a 5 nm thin film pushes a larger fraction of the electric field into the metal leading to more confined modes. The redistribution of the electric field from dielectric to metal is more significant for silver explaining the overall better performance of the vdWH metals for the thin film geometry. Experimental data for the Ag surface plasmon was adapted from Ref. [21]

generally yield more reliable band energies[26]. The primary effect of the HSE is to increase the size of the two gaps around the intermediate metallic band by around 0.5 eV (see Fig. S11) compared to PBE. This blue shifts the onset of interband transitions resulting in a significantly larger plasma frequency and lower losses. Consequently, the calculated plasmon propagation lengths and lifetimes becomes comparable to the noble metals while maintaining a small mode width (Fig. 4(f-h)).

Band structure engineered layered metals. With the goal of identifying new materials with band structures similar to those of 2H-TaS₂ and 2H-NbS₂, we have considered the class of layered materials of the form 2H-MXY (Fig. 5(a)), where M is a group 3 transition metal

(Ti,Zr,Hf), X is oxygen or a chalcogen (O,S,Se) and Y is a halogen (Cl,Br,I). While conserving the total electron number, the lower electronegativity of the group 3 compared to group 4 transition metals and the higher electronegativity of the halides compared to chalcogens, should increase the gap between the bands below and above the intermediate metallic band, which are composed mainly of chalcogen *p* and metal *d*, respectively. This should blue shift the interband transitions and decrease optical losses.

The calculated formation energies of the MXY compounds range from -2.53 eV to -0.92 eV per atom relative to the standard states. To check thermodynamic stability against other competing phases we compare the forma-

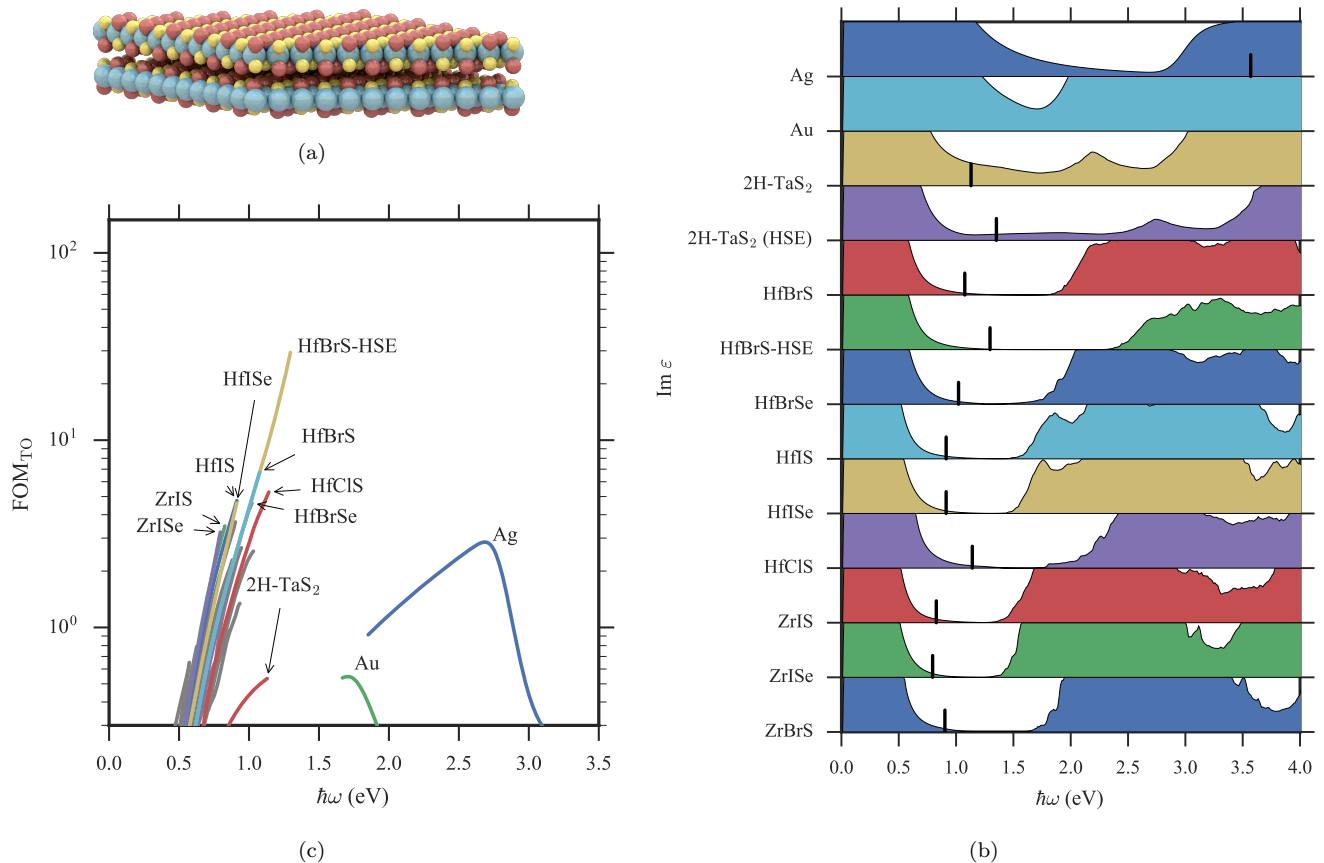


FIG. 5. **Optical properties of layer transition metal chalcogen-halogens.** Layered materials of the form 2H-MXY (a) where M is a group 3 transition metal, X is oxygen or a chalcogen (S, Se) and Y is a halogen (Cl, Br, I) are proposed as new plasmonic metals. The optical losses (b) shows that many of these compounds have considerable spectral ranges of low optical losses both compared to silver and to 2H-TaS₂ (the losses are normalized so that they can be directly compared between different materials). This is due to the decreased electronegativity of (Hf, Zr, Ti) compared to Ta which increases the gap below the Fermi level. As a result, the predicted FOM (c) is orders of magnitude better than silver in the near infrared.

tion energies to the convex hull, see Figure S5. Out of the 27 compounds, 19 are found to be stable while the rest are only weakly unstable with formation energies lying less than 50 meV above the convex hull. The structural stability of the chalo-halides was checked by performing relaxations of the monolayers in supercells containing 2 primitive cells (containing 12 atoms). With initial random distortions, the atoms relaxed back to restore the symmetry of the hexagonal lattice indicating that the structures are at least locally stable. The DFT calculations were performed fully spin polarised, but all the materials converged to a non-magnetic ground state.

The calculated $\text{Im}\epsilon$ are presented in Figure 5(b), and are characterized by significantly lower optical losses in the NIR regime 1-1.5 eV; a direct signature of the reduction in the density of states for scattering (Fig. S2). Figure 4 shows that the lowered optical losses entail an improved plasmon propagation length and lifetime as compared to 2H-TaS₂ for one of the compounds that exhibit the lowest optical losses, 2H-HfBrS, in both the

single interface and thin-film geometries. As we found for 2H-TaS₂, the HSE functional increases the band gaps of the MXY compounds by approximately 0.5 eV which reduces the losses even further and increases the plasma-frequencies, as illustrated for HfBrS (Fig. 5(b)). In the thin-film geometry this results in significantly improved plasmon lifetimes as compared to silver in the technologically important NIR frequency range (Fig. 4(g)) while maintaining a small mode volume (Fig. 4(h)).

Transformation optics. We now turn to an assessment of the potential of the layered metals for transformation optics (TO). Here the goal is to engineer the propagation of a wavefront through the volume of a metamaterial[22] for various applications. For a metamaterial structure containing metal-dielectric interfaces it is required that the metallic response ($\text{Re}\epsilon_M$) is compensated by the dielectric response ($\text{Re}\epsilon_D$) while losses remaining low. Consequently, the typical figure of merit for TO applications is $\text{FOM}_{\text{TO}} = 1/\text{Im}\epsilon_M$ while $-\text{Re}\epsilon_M \approx \text{Re}\epsilon_D$ [22]. Assuming that the metallic response can al-

ways be matched by a dielectric within the range $1 < \text{Re}\epsilon_D < 20$, the relevant FOM becomes

$$\text{FOM}_{\text{TO}} = \frac{1}{\text{Im}\epsilon_M} \theta(-\text{Re}\epsilon_M) \theta(\text{Re}\epsilon_M + 20) \quad (5)$$

where $\theta(x)$ is the Heaviside step function. Figure 5(c) shows the calculated FOM for the MXY-compounds and the best of the 18 metallic TMDs identified in Ref. [20] (see Sec. S1 for the full list of materials). Reassuringly the best TMD turns out to be 2H-TaS₂ which is one of the metals with an intermediate metallic band. In general, the losses in the TMDs increase from sulphides to selenides to tellurides due to a lowering of the onset of interband transition. A similar trend is known for the semi-conducting TMDs where the band gaps decrease when progressing through the chalcogenide group towards higher atomic number[27]. All the MXY compounds outperform both 2H-TaS₂ and the noble metals in the technologically important near-infrared frequency range. The improved performance is attributed to the larger gaps surrounding the intermediate metallic band which increases the plasma frequency and extends the loss-less regime between the intraband and interband transitions, see Figure 5(b).

Loss-less layered halides. Motivated by the excellent plasmonic properties of the (thermodynamically unstable) 1T-AlCl₂, we have performed a systematic study of layered bulk halides of the form (1T, 2H)-AY₂ where *A* is a group 3-13 element and *Y* is a halogen (Cl, Br or I). After filtering out materials with positive formation energies and finite magnetic moments and examining the band structures of the remaining materials we identify several candidates with close to perfect resemblance with the 'elusive loss-less material'. For example, 1T-GaCl₂ (see Fig. S8) has an isolated intermediate metallic band of width 1.0 eV, and an interband edge of 2.6 eV, a plasma frequency of 1.4 eV (Fig. S9). As a result the calculated plasmon propagation length and FOM_{TO} are essentially infinite (Fig. S10). Unfortunately, these halides are unlikely to be thermodynamically stable when considering other competing phases, although we have not explored this systematically. Nevertheless, we find it interesting that these metastable structures exhibit such extreme properties.

DISCUSSION

A critical issue for the layered metals considered in this work is stability. Even though most of the chalcogenides were found to be thermodynamically stable relative to other competing phases involving the same elements, the materials could oxidize and disintegrate when exposed to air or moisture. Whether this will happen is largely a matter of kinetics and a theoretical assessment requires calculation of reaction barriers which is beyond

the present study. However, we note that encapsulation could be a way to protect the materials from reacting with other species. For example, it was recently demonstrated that encapsulation in hexagonal boron-nitride can protect and stabilize phosphorene in air, which in its free form is highly unstable and oxidizes quickly ([28]). Airtight encapsulation of sensitive materials are routinely used in other fields such as organic light emitting diodes where the organic layer is sealed between glass plates.

A potential problem that pervades all narrow band metals is the risk of a phase-transition to magnetic-, charge density wave-, or Mott-insulating ground states. Such phase-transitions are often driven by a high density of states at the Fermi level. Thus the ideal metallic band for plasmonics should be wide enough to avoid such phase transitions and narrow enough to separate the intraband transitions from the interband transitions. Our calculations indicate that the chalcogenides are stable towards local structural distortions, but do not rule out the possibility of charge density wave-like distortions with larger periodicity. In fact, some of the metallic TMDs are known to exhibit charge density waves at low temperatures. On the other hand, at room temperature the presence of these phases is not expected to influence the optical properties that are governed by the gross features of the electronic structure. Moreover, the band width of the chalcogenides are comparable to those of the TMDs (see Figure 5(b)) which are known to behave as normal metals at room temperature, even for few layer samples[29].

Finally, we point to an added benefit of the vdW metals proposed in this work. Namely, their 2D nature allow them to be stacked with other non-metallic 2D materials like MoS₂ or hexagonal boron-nitride, to produce van der Waals metamaterials with ultra thin layer thickness and atomically well defined interfaces. We stress that it is very likely that the van der Waals metals proposed here should exhibit a lower scattering strength (controlled by the parameter *a* in Eq. (3)) compared to conventional metals like silver and gold. Indeed, the noble metals primarily used in plasmonics, exhibit relatively high losses arising from intraband transitions via scattering on surface and interface roughness[11, 30–32]. In contrast, the 2D materials form highly crystalline interfaces thus lowering the concentration of interfacial defects in actual devices. Combined with their intrinsic low-loss nature, this opens new perspectives for the fields of plasmonics and optical metamaterials.

METHODS

Electronic structure code

All electronic structure calculations have been performed with GPAW[33, 34] employing a plane wave basis sets and, unless explicitly stated, the PBE xc-functional.

The linear response optical properties were calculated on top of PBE ground states using the random phase approximation (RPA) for the density response function. The k-point integration required in the calculation of the response function was performed using the linear tetrahedron interpolation scheme[35]. Local field effects were included in all calculations of the optical response but were found to be unimportant. Spin-orbit coupling is shown in Sec. S6 to be negligible.

Band structures

The bandstructures of 2H-TaS₂ (ICSD ID: 651092), 3R-NbS₂ (ICSD ID: 645309) and 1T-AlCl₂ (AlCl₃ ICSD ID: 155670) were calculated with a plane wave cutoff of 600 eV and a k-point density of 10 Å⁻¹. In case of 1T-AlCl₂ (derived from AlCl₃) we determined the out-of-plane lattice constant to be 5.9 Å from structural relaxations using the optB88-vdW functional.

Relaxation of layered compounds

The out-of-plane lattice constant of all the layered materials were determined using the optB88-vdW functional. A plane wave cutoff of 600 eV was used when relaxing unless the compound contained oxygen in which case a cutoff of 900 eV was used. This approach was found to reproduce the experimental interlayer binding distance of 2H-TaS₂ to within 1%, see Fig. S3. The relaxed out-of-plane lattice constant of all the MXY components are presented in Fig. S4.

Supercell calculations of defects

Optical response calculations reported in Figure 3 employed supercells of 3 × 3 × 3 and 3 × 3 × 2 primitive cells for silver and 1T-AlCl₂, respectively. For silver a Monkhorst-Pack k-point sampling of 30 × 30 × 30 was employed and for 1T-AlCl₂ we used a sampling of size (24 × 24 × 16). A plane wave cutoff of 400 eV was employed in both response calculations. States up to at least 50 eV above the Fermi energy were included in the sum over states. These parameters were found to be sufficient for convergence of the optical response.

Optical response of known TMDs

In calculating the optical response of the layered metals identified in Ref. [20] (Fig. 4) we employ a plane wave cutoff of 600 eV and a Monkhorst-Pack k-point density of at least 30 Å⁻¹. States up to 40 eV above the Fermi energy were included in the sum over states. These settings were sufficient to converge the optical properties.

Surface plasmon propagation

Surface plasmons on uniaxial substrates have been analysed in Ref. [36]. They show that in the case of purely real dielectric functions the single interface surface plasmon polaritons (Fig. 4) exist only if $\epsilon_{\parallel} < 0$ and either $\epsilon_{\parallel}\epsilon_{\perp} > \epsilon_D^2$ or $\epsilon_{\perp} > \epsilon_D$ where ϵ_D is the dielectric function

of the dielectric and ϵ_{\parallel} and ϵ_{\perp} are respectively the in-plane and out-of-plane component of the dielectric tensor of the uniaxial material. The curves in Fig. 4(b-d) are only shown when the real parts of the dielectric functions fulfill one of these requirements.

For the IMI waveguide the surface plasmon modes have been determined using the method of Ref. [37]. For TM-polarized modes in uniaxial waveguides the dispersion relations to be solved become

$$L+ : \quad \epsilon_{M,\parallel}k_{\perp,D} + \epsilon_D k_{\perp,M} \tanh\left(\frac{-ik_{\perp,M}d}{2}\right) = 0 \quad (6)$$

$$L- : \quad \epsilon_{M,\parallel}k_{\perp,D} + \epsilon_D k_{\perp,M} \coth\left(\frac{-ik_{\perp,M}d}{2}\right) = 0 \quad (7)$$

for the antisymmetric (L+) and the symmetric (L-) modes with respect to the tangential electric field. Here $k_{\perp,M} = \sqrt{\epsilon_{\parallel}\omega^2/c^2 - \epsilon_{\parallel}k_{\parallel}^2/\epsilon_{\perp}}$ and $k_{\perp,D} = \sqrt{\epsilon_D\omega^2/c^2 - k_{\parallel}^2}$ are the wave vector components perpendicular to the metal-insulator interface in the metal and dielectric, respectively.

HSE06 calculations

The HSE06 calculations were performed non-self consistently on top of PBE. In case of 2H-TaS₂, the HSE06 calculation employed a gamma-centered Monkhorst Pack k-point sampling of (22, 22, 6) and a plane wave cutoff of 600 eV. For HfBrS we used a gamma-centered Monkhorst Pack k-point sampling of (8, 8, 4) and a plane wave cutoff of 600 eV.

HSE response calculations

For 2H-TaS₂ we found that a scissor operator of 0.55 eV on both gaps reproduced the DOS calculated by HSE (Fig. S11). For HfBrS we found that scissor operators of 0.7 eV and 0.5 eV on the lower and upper gaps, respectively, was sufficient to reproduce the DOS of HSE. We calculated the HSE response by applying the scissor operators to the PBE ground states using the PBE transition matrix elements.

Stability of MXY-compounds and halides

The monolayer stability of the transition metal chalcogen-halogen (MXY) compounds was evaluated based on the convex hull of the competing phases. The competing phases were determined using the Open Quantum Materials Database (OQMD) and includes 2-4 different structures in addition to the elemental phases. The heat of formation of the MXY compounds and all the competing phases were calculated using the fitted elemental phase reference energies (FERE) for the standard states [38]. A Monkhorst-Pack k-point sampling of (7, 7, 3) and a plane wave cutoff of 800 eV was employed and found to be sufficient for converging the total energy. The computed hull energies and heats-of-formation are presented in Table SII and Fig. S5.

Optical properties of MXY compounds

The optical properties of the MXY compounds from which the FOM was determined (Fig. 5) were calculated using a plane wave cutoff of 600 eV, a gamma-centered Monkhorst-Pack k-point sampling of size (18, 18, 8) and 300 bands (100 occupied) which was found to be sufficient for converging the optical properties. The optical response of the MXY compounds is anisotropic so the presented dielectric functions shows the average of the in-plane coefficients. This does not give rise to essential differences when comparing to specific components of the dielectric tensor.

ACKNOWLEDGEMENTS

The authors gratefully acknowledge the financial support from the Center for Nanostructured Graphene (Project No. DNRF103) financed by the Danish National Research Foundation.

The project received funding from the European Unions Horizon 2020 research and innovation program under grant agreement no. 676580 with The Novel Materials Discovery (NOMAD) Laboratory, a European Center of Excellence.

AUTHOR CONTRIBUTIONS

M.G. performed calculations and the data analysis under the supervision of K.S.T except for calculations of stabilities which were performed by M.P. The first draft of the paper was written by M.G.

-
- [1] Shalaev, V. M. *et al.* Negative index of refraction in optical metamaterials. *Optics letters* **30**, 3356–3358 (2005).
- [2] Zhaowei Liu *et al.* Far-Field Optical Superlens. *Nano Letters* **7**, 403–408 (2007).
- [3] Melville, D. & Blaikie, R. Super-resolution imaging through a planar silver layer. *Optics express* **13**, 2127–2134 (2005).
- [4] Kawata, S., Ono, A. & Verma, P. Subwavelength colour imaging with a metallic nanolens. *Nature Photonics* **2**, 438–442 (2008).
- [5] Linic, S., Christopher, P. & Ingram, D. B. Plasmonic-metal nanostructures for efficient conversion of solar to chemical energy. *Nature Materials* **10**, 911–921 (2011).
- [6] Atwater, H. A. & Polman, A. Plasmonics for improved photovoltaic devices. *Nature Materials* **9**, 865–865 (2010).
- [7] Shalaev, V. M. Transforming Light. *Science* **322**, 384–386 (2008).
- [8] Pendry, J. B., Schurig, D. & Smith, D. R. Controlling Electromagnetic Fields. *Science* **312**, 1780–1782 (2006).
- [9] Leonhardt, U. Optical conformal mapping. *Science* **312**, 1777–1780 (2006).
- [10] Khurgin, J. B. How to deal with the loss in plasmonics and metamaterials. *Nature Nanotechnology* **10**, 2–6 (2015).
- [11] Boltasseva, A. & Atwater, H. A. Low-Loss Plasmonic Metamaterials. *Science* **331**, 290–291 (2011).
- [12] Tassin, P., Koschny, T., Kafesaki, M. & Soukoulis, C. M. A comparison of graphene, superconductors and metals as conductors for metamaterials and plasmonics. *Nature Photonics* **6**, 259–264 (2012).
- [13] Arnold, M. D. & Blaber, M. G. Optical performance and metallic absorption in nanoplasmonic systems. *Optics express* **17**, 3835–47 (2009).
- [14] Blaber, M. G., Arnold, M. D. & Ford, M. J. Designing materials for plasmonic systems: the alkaline intermetallics. *Journal of Physics: Condensed Matter* **22**, 95501 (2010).
- [15] Naik, G. V. *et al.* Titanium nitride as a plasmonic material for visible and near-infrared wavelengths. *Opt. Mater. Express* **2**, 478–489 (2012).
- [16] Naik, G. V., Shalaev, V. M. & Boltasseva, A. Alternative plasmonic materials: Beyond gold and silver. *Advanced Materials* **25**, 3264–3294 (2013).
- [17] Chen, J. *et al.* Optical nano-imaging of gate-tunable graphene plasmons. *Nature* **487**, 77 (2012).
- [18] Fei, Z. *et al.* Gate-tuning of graphene plasmons revealed by infrared nano-imaging. *Nature* **487**, 82–85 (2012).
- [19] Khurgin, J. B. & Sun, G. In search of the elusive lossless metal. *Applied Physics Letters* **96**, 2012–2015 (2010).
- [20] Lebègue, S., Björkman, T., Klintonberg, M., Nieminen, R. M. & Eriksson, O. Two-dimensional materials from data filtering and Ab Initio calculations. *Physical Review X* **3**, 1–7 (2013).
- [21] Brown, A. M., Sundararaman, R., Narang, P., Goddard, W. A. & Atwater, H. A. Nonradiative Plasmon Decay and Hot Carrier Dynamics: Effects of Phonons, Surfaces, and Geometry. *ACS Nano* **10**, 957–966 (2016).
- [22] West, P. R. *et al.* Searching for better plasmonic materials. *Laser and Photonics Reviews* **4**, 795–808 (2010).
- [23] Ozbay, E. Plasmonics: Merging Photonics and Electronics at Nanoscale Dimensions. *Science* **311**, 189–193 (2006).
- [24] Pitarke, J. M., Silkin, V. M., Chulkov, E. V. & Echenique, P. M. Theory of surface plasmons and surface-plasmon polaritons. *Reports on Progress in Physics* **1**, 54 (2006).
- [25] Yan, J., Jacobsen, K. W. & Thygesen, K. S. Conventional and acoustic surface plasmons on noble metal surfaces: A time-dependent density functional theory study. *Physical Review B* **86**, 241404 (2012).
- [26] Krukau, A. V., Vydrov, O. A., Izmaylov, A. F. & Scuseria, G. E. Influence of the exchange screening parameter on the performance of screened hybrid functionals. *The Journal of Chemical Physics* **125**, 224106 (2006).
- [27] Rasmussen, F. A. & Thygesen, K. S. Computational 2D Materials Database: Electronic Structure of Transition-Metal Dichalcogenides and Oxides. *Journal of Physical Chemistry C* **119**, 13169–13183 (2015).
- [28] Pei, J. *et al.* Producing air-stable monolayers of phosphorene and their defect engineering. *Nature Communications* **7**, 10450 (2016).
- [29] Zhao, S. *et al.* Two-dimensional metallic NbS₂: growth, optical identification and transport properties. *2D Materials* **3**, 25027 (2016).

- [30] Dionne, J. A. & Atwater, H. A. Plasmonics: Metal-worthy methods and materials in nanophotonics. *MRS Bulletin* **37**, 717–724 (2012).
- [31] Wu, Y. *et al.* Intrinsic optical properties and enhanced plasmonic response of epitaxial silver. *Advanced Materials* **26**, 6106–6110 (2014).
- [32] Fedotov, V. A., Uchino, T. & Ou, J. Y. Low-loss plasmonic metamaterial based on epitaxial gold monocrystal film. *Optics express* **20**, 9545–9550 (2012).
- [33] Yan, J., Mortensen, J. J., Jacobsen, K. W. & Thygesen, K. S. Linear density response function in the projector augmented wave method: Applications to solids, surfaces, and interfaces. *Physical Review B* **83**, 245122 (2011).
- [34] Enkovaara, J. *et al.* Electronic structure calculations with GPAW: a real-space implementation of the projector augmented-wave method. *Journal of physics: Condensed matter* **22**, 253202 (2010).
- [35] MacDonald, A. H., Vosko, S. H. & Coleridge, P. T. Extensions of the tetrahedron method for evaluating spectral properties of solids. *Journal of Physics C: Solid State Physics* **12**, 2991–3002 (1979).
- [36] Warmbier, R., Manyali, G. S. & Quandt, A. Surface plasmon polaritons in lossy uniaxial anisotropic materials. *Phys. Rev. B* **85**, 85442 (2012).
- [37] Dionne, J. A., Sweatlock, L. A., Atwater, H. A. & Polman, A. Planar metal plasmon waveguides: frequency-dependent dispersion, propagation, localization, and loss beyond the free electron model. *Phys. Rev. B* **72**, 75405 (2005).
- [38] Stevanovic, V., Lany, S., Zhang, X. & Zunger, A. Correcting density functional theory for accurate predictions of compound enthalpies of formation: Fitted elemental-phase reference energies. *Physical Review B - Condensed Matter and Materials Physics* **85**, 115104 (2012).